Combustion and Flame 162 (2015) 2256–2271

Contents lists available at ScienceDirect

Combustion and Flame

journal homepage: www.elsevier.com/locate/combustflame

Rate-Controlled Constrained Equilibrium (RCCE) simulations of turbulent partially premixed flames (Sandia D/E/F) and comparison with detailed chemistry

Salem Elbahloul, Stelios Rigopoulos *

Department of Mechanical Engineering, Imperial College London, Exhibition Road, South Kensington, London SW7 2AZ, UK

ARTICLE INFO

Article history:
Received 30 September 2014
Received in revised form 23 January 2015
Accepted 26 January 2015
Available online 11 March 2015

Keywords:
RCCE
Reduced chemistry
Turbulent flames
PDF methods

ABSTRACT

This paper investigates the potential of the RCCE mechanism reduction approach for modelling turbulent flames within the framework of transported PDF methods. For this purpose, PDF simulations are performed with an RCCE-reduced mechanism via direct integration of the RCCE ODEs, without any tabulation, and comparison is made with both the experimental results and those from a PDF simulation with direct integration of the detailed mechanism. The flames simulated are the Sandia flames D/E/F and the simulations are carried out with a RANS approach and a Lagrangian particle method for solving the transported joint-scalar PDF equation. The detailed mechanism is the well known GRI 3.0 CH_4 combustion mechanism. The turbulence closure employed is the $k-\varepsilon$ model, while the micromixing closure in the PDF transport equation is the Interaction with the Mean (IEM) model. The RCCE-reduced mechanism incorporates 18 constraints, selected from the original 53 species based on laminar flamelet simulations. Excellent agreement was observed between the RCCE simulations and direct integration, indicating that the reduced mechanism can reproduce very well the features of the full mechanism. Agreement with experimental results is also very good, given the turbulence and mixing models employed.

© 2015 The Authors. Published by Elsevier Inc. on behalf of The Combustion Institute. This is an open access article under the CC BY license (http://creativecommons.org/licenses/by/4.0/).

1. Introduction

Transported probability density function (PDF) methods have long been advocated as a solution to the problem of turbulence–chemistry interaction modelling in turbulent reacting flows, due to their potential to accommodate complex chemistry involving several species with the reaction source term still appearing in closed form. Yet their application is faced by two main difficulties: the need for closure of the micromixing term and the extensive computational time required for the integration of the chemical kinetics ODEs for complex mechanisms. Efforts to address the first of these issues so far involved the development of advanced micromixing models such as EMST, mapping closures and multiple mapping conditioning (MMC), as well as the application of LES which reduces the impact of the micromixing model. Approaches to the solution of the second issue include mechanism reduction and tabulation approaches; indeed, it can be said that PDF methods have been a major driving force for the development of methods in this area.

From the onset of the use of transported PDF methods in combustion, researchers have sought to employ highly simplified mechanisms and tabulation methods. In a way, this seems to defy the purpose of employing PDF methods, since their main advantage is their ability to accommodate complex chemistry and turbulence–chemistry interaction by virtue of the source term appearing in closed form. Yet the extreme number of integrations of the chemistry ODEs required renders the direct integration of comprehensive mechanisms prohibitive. The earliest chemical models used in the context of PDF methods were very small mechanisms, comprising only a few steps and species. One of them was a global hydrocarbon 4-step mechanism [1] which, owing to the very small number of variables involved, could be tabulated via a straightforward interpolation table approach, and has been used in pdf studies such as [2]. Much early work on PDF methods was conducted with other highly reduced (4–5 steps) mechanisms, and examples of their application to turbulent non-premixed flames can be found in [3].

Another approach, developed in Pope's group with transported PDF methods in mind, is the In-Situ Adaptive Tabulation (ISAT) [4], which is a tabulation procedure performed in real-time (i.e. during the simulation). ISAT has been employed in conjunction with moderately reduced mechanisms (e.g. 16 species) in [5,6] to simulate

* Corresponding author.

http://dx.doi.org/10.1016/j.combustflame.2015.01.023
0010-2180/© 2015 The Authors. Published by Elsevier Inc. on behalf of The Combustion Institute.
This is an open access article under the CC BY license (http://creativecommons.org/licenses/by/4.0/).

turbulent diffusion flames including the Sandia flame D. The arrival of LES greatly increased the computational requirements, and highly reduced tabulated mechanisms were used even in fairly recent studies, such as a LES-PDF study of Sandia flame D [7] which still uses the global hydrocarbon 4-step mechanism [1]. A later LES-PDF study by the same group [8] used the ARM reduced mechanism [9], comprising 19 species.

All of the reduced mechanisms discussed so far were derived using the traditional methods of Quasi-Steady State Approximation (QSSA) and Partial Equilibrium (PEA). In deriving mechanisms via these concepts, the selection of species and the derivation of the equations describing the reduced mechanism have to be carried out individually for each reduced mechanism, based on knowledge and chemical insight. This was not a problem in the beginning, while the focus of research on PDF methods and their application was limited to a few simple fuels, such as hydrogen and methane. With mechanisms becoming more and more complex, however, and the recent interest in modelling combustion of complex fuels, this procedure has become more and more cumbersome. Systematic methods for investigating time scales and choosing the QSSA species were also developed, such as Computational Singular Perturbation (CSP) [10,11] and Level of Importance (LOI) [12]. More information on these and on other methods of mechanism reduction can be found in the review papers [13,14].

Rate-Controlled Constrained Equilibrium (RCCE) is a concept for deriving reduced mechanisms that can be regarded as an alternative to the traditional QSSA and PEA concepts. In RCCE, a subset of chemical kinetics involving the major species is employed to drive the integration, while a set of algebraic equations derived from the minimisation of the free energy, but pertaining only to the minor species, are used to close the ODE system. A major advantage of RCCE is that the choice of major and minor species enters the equations as a parameter, so that various reduced mechanisms can be derived and tested automatically. The choice of species to be retained can be made on the basis of the same concepts used in traditional reduced mechanisms, such as heuristics and investigation of the magnitude of species' concentrations across the flame. At the same time, RCCE potentially lends itself to easy integration with systematic procedures that produce an ordering of species, such as CSP and LOI, as it can accept the ordered list of major species as external input.

The basic concept of RCCE was initially proposed by Keck and Gillespie ([15], see also [16]) in the context of homogeneous combustion, but their work was not followed up for a long time, with the exception of the work of Yousefian [17] on the relationship of RCCE and PEA. The work by our group on RCCE begun with developing numerical methods for RCCE in homogeneous combustion [18], and continued with coupling RCCE with flow problems, starting with laminar non-premixed [19] and premixed flames [20,21]. The recent interest in RCCE has resulted in several other works: [22] also investigates homogeneous combustion of monocarbon fuels, while in [23] RCCE is combined with ISAT and applied to laminar premixed and non-premixed flames. In [24], the RCCE-ISAT methodology is tested on a partially stirred reactor, and the focus is on the selection of constraints using the Greedy Algorithm with Local Improvement (GALI). Recently, RCCE has also been applied to some turbulent flames via CMC [25,26] and via PDF but tabulated through Artificial Neural Networks (ANNs) [27]. Another application of RCCE to turbulent flames has been in conjunction with ISAT [28,29].

In all of these cases, however, RCCE was employed in the context of various tabulation approaches that introduce additional approximations, and the focus of the studies has been on the evaluation of the combined approach. E.g. the focus of [27] was on the errors associated with the ANN tabulation, while [29] deals with the issue of effective distribution of the CPU load associated with chemistry computations in large-scale parallel simulations. The question whether RCCE, in its original form, is capable of producing results approximating the detailed mechanism, has not been addressed other than in the context of simplified problems. On the other hand, reasonably sized QSSA-derived mechanisms have been investigated via real-time direct integration in the context of PDF methods (e.g. [30] including 14 independent scalars).

Therefore, the objective of the present paper is to address this question by coupling both RCCE and direct integration of a detailed mechanism with a RANS-PDF approach and simulating a set of turbulent partially premixed flames. Both the reduced mechanism and the detailed mechanism are employed without any tabulation, and while comparison with experiments is also made, the focus is on the comparison of RCCE with direct integration. It must be stressed that the development of RCCE was not done with this purpose in mind: real-time PDF computations are always expensive, even with reduced mechanisms. The main function of mechanism reduction in the context of PDF methods is the reduction of dimensionality, in order to render the mechanism suitable for tabulation. However, an investigation of the real-time integration of the original RCCE equations coupled with a PDF method with no additional concepts is, in our point of view, an essential step that must be taken towards the wider application of the RCCE concept in the context of tabulation approaches.

Both the chemistry and the test problem were chosen to be as standard as possible: the detailed mechanism is the well-known GRI 3.0 and the problem is the set of Sandia flames D/E/F that have long served as the benchmark for the turbulence combustion community. Although LES-based simulations of turbulent flames are now common, the performance of RANS-PDF methods in capturing the interaction of mixing and reaction is well known and therefore they constitute a good basis for comparing RCCE and direct integration of the detailed mechanism.

The number of previous simulations of Sandia flames is very high, and we will only mention here a few that have certain elements in common with the methodology presented here (mostly studies employing PDF methods, although a few studies involving other methods will also be mentioned). The Sandia D/E/F flames have been computed with the joint PDF of the velocity, turbulent frequency and composition with an augmented reduced mechanism (ARM) by Tang et al. [31] and Xu and Pope [32] and later with the full GRI 3.0 mechanism by Cao et al. [33]. Lindstedt and coworkers [34,35] implemented the transported scalar PDF in the context of second moment closure of the flow field and applied it to flames B, D and F. Jaishree and Haworth [36] computed these flames with three different methods for solving the composition PDF equation in the context of the hybrid RANS-PDF approach: the Lagrangian particle method, the stochastic field method and, finally, the multi-environment MEPDF method which employs the Direct Quadrature Method of Moments (DQMOM) closure. In LES, Jones and Prasad [8] employed the stochastic field method for LES-PDF and computed the three flames (D, E and F) successfully. These flames have also been simulated with other turbulence–chemistry interaction models such as the flamelet and CMC – e.g. Pitsch and Steiner [37] implemented the flamelet model with LES and applied it to Flame D, and later Ihme and Pitsch [38] performed LES of flames D and E with the flamelet-progress variable model. The CMC model was also applied in the context of RANS, e.g. [39] and LES, e.g. [40,41].

The rest of the paper is structured as follows. First, a summary of RCCE and the RANS-PDF approaches is given, followed by details of the numerics employed in this study. Results are then shown for the three Sandia flames, and various aspects of the RCCE/direct integration simulations are discussed.

2. Rate-Controlled Constrained Equilibrium (RCCE)

2.1. The RCCE concept

A brief description of RCCE will be given here; for more details, particularly on the derivation of the equations in the formulation employed here, one is referred to [19,20]. The equilibrium concentration of a chemical mixture can be determined in two ways: the method of equilibrium constants, where every single reaction is put to equilibrium, and the minimisation of free energy, which is based on thermodynamic information and does not require knowledge of the mechanism. The latter concept is employed in RCCE, in conjunction with chemical kinetics, to compute the dynamical evolution of a chemical system featuring a separation of time scales. In that case, the species exhibiting fast time scales can be regarded as equilibrated compared to the others and can be computed by a constrained minimisation of the free energy - constrained by the concentrations of the major species that are controlled by the kinetics. In RCCE the dynamics of the system are led by a sub-set of the chemical kinetics ODEs from the original mechanism, but the equilibrated species are calculated by a set of algebraic equations arising from the minimisation of the free energy, which define a manifold of constrained equilibrium states and force the system to remain there.

2.2. Chemical kinetics equations

We first introduce the notation that will be employed for the chemical kinetics in the detailed mechanism. Consider a chemical reaction mechanism featuring N_e atomic elements, N species and N_r reactions. Its dynamical evolution is described by a set of differential equations in terms of the reaction rates of individual reactions, r_k, and the stoichiometric factors, v_{jk}, as follows:

$$\frac{dn_j}{dt} = \sum_{k=1}^{N_r} v_{jk} r_k(n_1, n_2, \ldots, n_N, T, \rho) \quad (j = 1, 2, \ldots, N) \tag{1}$$

together with the algebraic equations:

$$\sum_{j=1}^{N} n_j h_j^o(T) = h \tag{2}$$

$$\sum_{j=1}^{N} n_j \rho RT = P \tag{3}$$

Here n_j denotes the concentrations of chemical species in kmol per unit mass of the mixture, a notation especially suited to variable density gas flows, while h is the enthalpy of the mixture per unit mass and $h_j^o(T)$ is the enthalpy of each species (both formation and thermal). The reaction rates are related to the concentrations by the law of mass action and to the temperature by the Arrhenius equation.

2.3. RCCE equations

The equations describing the constrained equilibrium state can be derived from the following considerations: just as the equilibrium of a chemical reaction in a closed system at fixed temperature can be computed via minimisation of the free energy (Gibbs or Helmholtz), it is possible to define a further equilibrium condition for fixed temperature, pressure and concentrations of the leading species. E.g. suppose that we have a CH_4–O_2 system and we constrain O_2. Then all the O-atoms will occur in the form of O_2, but the C and H atoms may be packed into whichever molecules are thermodynamically stable under these conditions. The RCCE equations are derived by minimising the Gibbs free energy, g, subject to the conservation of the elements, enthalpy, mass and constrained species (hereafter N_c). To perform the minimisation with the method of Lagrange multipliers, we introduce the parameters λ_i^e – Lagrange multipliers that are called element potentials, as well as the additional parameters λ_i^c, which we call constraint potentials. The following system of equations can be derived for the manifold of constrained equilibrium states [20]:

$$\mu_j^o + RTln\frac{n_j}{n} + RTln\frac{P}{P_o} + \sum_{i=1}^{N_e} \lambda_i^e a_{ij}^e + \sum_{i=1}^{N_c} \lambda_i^c a_{ij}^c = 0 \tag{4}$$

where a_{ij}^c and a_{ij}^e are the matrices that relate the constrained species and elements with the overall concentrations, and P_o, μ_j^o are the pressure and chemical potential at the standard state, respectively.

To calculate the dynamical evolution of the system, only the constraints need to be described by ODEs, taken directly from the detailed mechanism (Eq. (1)):

$$\frac{dC_i}{dt} = \sum_{j=1}^{N} a_{ij}^c \left[\sum_{k=1}^{N_r} v_{jk} r_k(n_1, n_2, \ldots, n_N, T, \rho) \right] \quad (i = 1, 2, \ldots, N_c) \tag{5}$$

These ODEs must be solved together with algebraic equations defining the manifold of constrained equilibrium states. The latter are derived from Eq. (4) by taking exponentials, so that the resulting equations yield explicitly the composition at the manifold:

$$n_j^* = n\frac{P^o}{P} exp\left(\frac{-\mu_j^o}{RT}\right) exp\left[\sum_{i=1}^{N_e}\left(a_{ij}^e \lambda_i^e\right)\right] exp\left[\sum_{i=1}^{N_c}\left(a_{ij}^c \lambda_i^c\right)\right] \quad (j = 1, \ldots, N) \tag{6}$$

together with the algebraic equations expressing conservation of elements, enthalpy, pressure and consistency with constraints.

The final set of equations form a differential–algebraic (DAE) problem, the dependent variables being the species, Lagrange multipliers, temperature and density. Only the species associated with the slow time scales, the temperature and the pressure need to be known to initiate the computation; the remaining variables are internal. Initial conditions must be specified for the constraints; the Lagrange multipliers and constrained equilibrium composition can be calculated by solving the constrained equilibrium algebraic equations at the initial state. A consistent definition of constraints must not allow the initial conditions to be modified. Finally, it must be noted that an equivalent implicit ODE system can be derived that computes the evolution of the system in terms of the Lagrange multipliers, temperature and density, which is usually more efficient for numerical implementation, and is employed here; for more information the reader is referred to [19,20]. It must be emphasised that the equations of RCCE are general, and the selection of constrained and equilibrated species appears only as a parameter via the matrix a_{ij}^c. This fact greatly facilitates the investigation of reduced systems.

3. Joint-scalar transported PDF modelling of turbulent reacting flows

3.1. RANS equations and turbulence modelling

The basis for the PDF method employed in this study are the RANS equations supplemented with a turbulence model, which provide the mean velocity field and turbulence quantities for the joint-scalar PDF transport equation. While LES-PDF simulations have appeared in the literature and, in general, LES simulations of turbulent combustion perform better as the impact of the mixing model is minimised, the focus of this study is on the comparison of RCCE and direct integration rather than on producing the

best possible simulation of the Sandia flames. The shortcomings of RANS-PDF methods in simulating the mixing field are known and are also exhibited by the results shown in this study. For variable density flows, the Favre-averaged equations are employed; they are not shown here, since they can be found in many sources (e.g. [2]). The popular (k–ε) model is employed for turbulence modelling; its formulation in the standard form was originally proposed by Jones and Launder [42,43].

3.2. Joint-scalar PDF transport equation

The transported joint-scalar PDF is a function that contains all one-point statistical information about the scalar field:

$$f(y_\alpha; x_i, t)$$

As with everything else, for variable density flows the PDF must be Favre-averaged:

$$\widetilde{f}(y_\alpha; x_i, t) = \frac{1}{\langle\rho\rangle}\int_{\rho_{min}}^{\rho_{max}} \langle\rho\rangle\, f(y_\alpha; x_i, t) d\rho \tag{7}$$

where ρ is the mean density.

The transport equation for the joint-scalar PDF can be derived from the instantaneous conservation equations in several ways, of which the most well-known is taking the ensemble average of the fine-grained density [44–46]. The equation can be written in the following form:

$$\begin{aligned}&\frac{\partial\langle\rho\rangle\widetilde{f}}{\partial t} + \frac{\partial}{\partial x_i}\left(\langle\rho\rangle\widetilde{u_i}\widetilde{f}\right) + \langle\rho\rangle\frac{\partial}{\partial y_\alpha}\left(\dot{\omega}_\alpha\widetilde{f}\right)\\ &\quad = -\frac{\partial}{\partial x_i}\left(\langle\rho\rangle\langle u_i'' \mid y_\alpha = \psi_\alpha\rangle\widetilde{f}\right) + \frac{\partial}{\partial y_\alpha}\left(\left\langle\frac{\partial J_{i,\alpha}}{\partial x_i}\middle| y_\alpha = \psi_\alpha\right\rangle\widetilde{f}\right)\end{aligned} \tag{8}$$

Here, $\widetilde{u_i}$ is the Favre averaged mean velocity and $\langle u_i'' \mid y_\alpha = \psi_\alpha\rangle$ is the conditional velocity fluctuation. ψ_α is the sample space variable for scalar y_α. The micromixing term is written in terms of the diffusion flux, $J_{i,\alpha}$. The chemical source term $\dot{\omega}_\alpha$ for production of reactive species and other non-conserved scalars can be expressed in exact form; this is the most advantageous feature of transported pdf methods.

The unclosed terms in the PDF transport equation are the terms on the right-hand side which represent, respectively, turbulent transport in physical space (turbulent diffusion) and micromixing in scalar space. The turbulent transport term is unclosed because the joint-scalar PDF does not include information on velocity statistics. When an eddy-diffusivity model is applied for the flow field, this term is commonly modelled using a gradient diffusion assumption:

$$\frac{\partial}{\partial x_i}\left(\langle\rho\rangle\langle u_i'' \mid y_\alpha = \psi_\alpha\rangle\widetilde{f}\right) = -\frac{\partial}{\partial x_i}\left(\langle\rho\rangle\frac{\nu_t}{\sigma_t}\frac{\partial\widetilde{f}}{\partial x_i}\right) \tag{9}$$

where ν_t and σ_t are the eddy viscosity (to be computed from the turbulence model) and turbulent Schmidt number, respectively. The micromixing term also requires modelling and represents the main closure difficulty in transported PDF methods. This term represents the processes responsible for the evolution of the scalar fields by mixing occurring at the small scales. In this paper we employ the Interaction with the Mean (IEM) model [47,48], whose principle is to perform mixing of the individual entities of the PDF by allowing their properties to interact with their local ensemble means.

3.3. Lagrangian particle method for solution of the RANS-PDF equations

The numerical approach employed here consists of a hybrid algorithm employing a finite volume CFD solution for the mean flow field, supplemented by a turbulence model, and a Lagrangian particle method for solving the PDF transport equation. The method has been discussed extensively e.g. in [45,49,46]. In this method, the increments of each physical process over a time step are computed sequentially using the operator splitting or fractional step method. The joint scalar PDF equation is represented by an ensemble of particles. Each particle carries a set of scalar variables y_α which includes composition and enthalpy. Velocity is interpolated at the particles locations from the cell centre values, which are provided by the Eulerian k–ε CFD solver. Particles move in the physical space according to a stochastic differential equation. The equation incorporates a deterministic convection (drift) component and a stochastic (diffusion) component and can be written as:

$$\delta x_i^p = \left(\tilde{u}_i + \frac{1}{\langle\rho\rangle}\frac{\partial\mu_t}{\partial x_i}\right)\delta t + \left(2\frac{\mu_t + \mu}{\langle\rho\rangle}\right)^{1/2}\delta W_i \tag{10}$$

where $\tilde{u}_i$ is the Favre mean velocity of the particle. The turbulent diffusivity μ_t is also obtained from the flow field CFD solver. The second term on the right hand side of Eq. (10) represents the stochastic diffusion process. δW_i is the increment of an isotropic Wiener process during the PDF time step and involves a normal random variable with zero mean and unity variance. δW is thus a random variable with zero mean and a variance equal to the PDF time step δt [49]. The evolution of the scalar fields by molecular mixing and reaction is performed by a fractional step method. The molecular mixing is treated by implementing the IEM model:

$$y_\alpha^p(t + \delta t) = y_\alpha^p(t) - \frac{C_y}{2}\frac{\varepsilon}{k}\left(y_\alpha^p(t) - \widetilde{y_\alpha}\right)\delta t \tag{11}$$

where C_y is the mixing time scale and $\widetilde{y_\alpha}$ is the local ensemble mean of the scalar variable y_α.

4. Numerical procedure

4.1. Experimental setup

The Sandia flames are piloted flames that have the same geometric configuration and composition of the jet, pilot and co-flow streams but differ in the jet and pilot velocities. The D, E, F flames are part of a series of six piloted partially premixed flames (A–F) which has been studied experimentally by Barlow and coworkers [50,51], who provided detailed measurements of the scalar fields. Laser Doppler Velocimetry (LDV) measurements for the flow field were published by Schneider et al. for the flames D, E and F [52]. The jet Reynolds numbers of the flames span from 1,100 (for the A which is a laminar flame) to 44,800 (for the F flame which is turbulent with global extinction and reignition).

The unconfined flames were established on a piloted burner setup which had been developed at Sydney University [53]. The burner has a nozzle diameter of $D = 7.2$ mm and a premixed pilot that extends to a diameter of 18.2 mm. The main fuel jet is a partially premixed methane–air mixture with composition of 25% CH_4 and 75% air by volume which produces non-sooty flames. The setup minimises the formation of soot and soot precursors, in order to facilitate the study of gas-phase chemistry and turbulent-chemistry interaction without having to incorporate models for radiation and soot formation. The pilot burns a lean ($\Phi = 0.77$) premixture of C_2H_2, H_2, O_2, CO_2, and N_2 with the same nominal enthalpy and equilibrium composition as methane–air at this equivalence ratio. The energy release of the pilot is approximately

6% of the main jet. Barlow and Frank stated that during the scalar field measurement the burner exit is set approximately 150 mm above the exit of a vertical wind tunnel, while during the flow field measurement by Schneider et al. [52] it was aligned 20 mm above the exit of the co-flow nozzle.

4.2. RANS-PDF simulation setup

The computational implementation of the RANS-PDF method is based on the work of di Veroli and Rigopoulos [54,55]. Their original implementation was developed for constant-density flows, so their code was modified to account for density variations in turbulent combustion flows. The flow field computations is done with the RANS code BOFFIN [56], which is a finite volume CFD solver. The equations of k and ε are in the standard form except for the well-known modification of $C_{\varepsilon 2}$ to 1.8 instead of 1.92 to correct the turbulent jet spread rate. The turbulent Schmidt or Prandtl number σ is taken to be 0.7. The Total Variation Diminishing (TVD) scheme developed by Van Leer [57] is applied to the convection terms, as it is known to give a second order accuracy for the differencing and prevents spatial oscillations. Cell face values which are required in the TVD scheme are obtained from an upwind interpolation with the correction and limiter of Van Leer [57].

The grid employed in this study is axisymmetric, orthogonal and non-uniform as it is generated with a moderate expansion ratio around [1.02] in both the axial and radial directions, in order to obtain finer resolution in the near-field region (i.e. near the jet and pilot nozzles). The solution domains for flames E and F was extended to 100 jet diameters ($100D$) in the stream-wise direction and 15 diameters ($15D$) in the radial direction and the grid has 100×80 orthogonal non-uniform cells in the axial and radial directions respectively. The solution domain of flame D has the same grid spacing of the other two flames but has only 70 cells in the stream-wise direction, which extends only up to ($55D$). A simulation for flame D with a $100D$-long grid (not presented here) showed that clipping the grid to $55D$ did not affect the results.

At the inlet boundary, the values of the dependent variables need to be specified explicitly. The detailed flowfield experimental data by Schneider et al. [52] include profiles at an axial distance of 1 mm from the jet exit, so the inlet profile for mean axial and radial velocity and turbulent kinetic energy can be taken from this data set. According to [52], turbulent kinetic energy is computed, with the assumption of axial symmetry, from axial and radial Reynold stress components. The dissipation rate ε is not explicitly provided and has to be carefully estimated. It can be approximated from the turbulent kinetic energy using the mixing length hypothesis to specify the mixing length [58]. There are many forms for the profile of the mixing length that can be applied for the turbulent fuel jet. Those that have been suggested in the literature include the ramping function of [59] ($l_m = min(\kappa y, 0.09R)$) where y is the distance from the nozzle wall. This form applies variation in mixing length with y only in the cells next to the wall when $y < 0.22R$. Both Nikuradse and Merci et al. [60] proposed alternative expressions which incorporate variation of the mixing length with y for all the jet radius (see Merci et al. [60]). Alternatively, constant mixing length assumption throughout the jet radius has also been used (e.g. [61] with $l_m = 0.075R$) and ε_{jet} would only vary with k. The latter constant l_m approximation has been used in this study. Finally, detailed species concentrations for the pilot of flame D were also provided by Barlow and Frank [62]. This measured pilot composition has been used in all computations of the three flames.

4.3. Chemical kinetics and selection of constraints

In this study, the determination of the set of constraints employed in the PDF simulation was determined via a series of laminar flamelet simulations with increasing numbers of constraints. As mentioned, one of the advantages of RCCE is that it greatly facilitates the investigation of reduced mechanisms, as one simply needs to change the specification of constraints externally (i.e. as an input to the code) without need to change the structure of the equations or the numerics. The laminar flamelet is an abstract problem with a strong similarity to turbulent diffusion flames, especially since one can vary the strain rate to generate conditions similar to what would result at extinction. The fuel and oxidant at the flamelet calculations were set to be the same as the composition of the inlets to the Sandia flames. All the sets of constraints employed here are global; although further refinement is possible via adaptive selection of constraints [63], the intention here was to examine the potential of a single global RCCE-reduced mechanism to capture the structure of these benchmark flames.

The successive improvement of the predictions for various sets of constraints is shown in Fig. 1. The seven most major species, i.e. $CH_4, O_2, CO_2, CO, H_2O, N_2, H_2$, as well as the important radicals H, OH and O formed the basis for the investigation. As no NO_x predictions will be attempted here, no further N-containing species were investigated. The three dominant C_2 species (C_2H_2, C_2H_4 and C_2H_6), as well as the radical CH_3, were also found to be essential and are present in most reduced CH_4 combustion mechanisms. These 14 constraints comprise the first set plotted in Fig. 1. At lower strain rate, this set produces very good results, but it extinguishes at higher strain. A 16-constraint set adding CH_2O and CH_3OH could maintain the flame at higher strain rate, but not close to extinction. Finally, the addition of CH_2 and $CH_2(s)$ reproduced well the extinction strain rate, as well as the structure of the flame across the whole range of strain rates. It must be noted that most of these species are included also in the well-known ARM reduced mechanism and its predecessors [64,65,9], and the size of the mechanism is also similar.

The actual number of scalars to be integrated in RCCE is 24 (18 species + 4 elements + 2 thermodynamic constraints). The CPU time required to integrate the RCCE-reduced mechanism per time step varied from about 40% to 60% of the time required for direct integration to sometimes being comparable. The low CPU gain is due to several factors; the degree of reduction is not great (about half the number of ODEs), and in addition GRI 3.0 is a very efficient, non-stiff mechanism; previous studies with a bigger and more stiff propane mechanism [21] indicated much higher CPU savings. However, it must be noted that any real-time integration of chemistry is costly for use in a PDF method; the main objective of applying RCCE is the reduction in the dimensionality so that the reduced mechanism may be tabulated, and mechanisms of around 20 species have be successfully tabulated via ANN [27].

5. Results and discussion

5.1. Flow field and mixture fraction predictions

The three flames have been computed with direct integration of the GRI 3.0 mechanism and with the 18-constraint RCCE reduced mechanism. Overall, the general characteristics of flow field of the three flames are reasonably well reproduced. The centreline mean mixture fraction is comparable up to $x = 30D$ but is considerably underpredicted at higher axial distances. In addition the initial radial spreading of the fuel (e.g. at $x = 7.5D$ and $x = 15D$) is overpredicted, which is likely to be due to either uncertainties in mixing modelling or overprediction of $\widetilde{k}$, which is used to calculate the apparent turbulent diffusivity for notional particles. The profiles of the mean axial velocity and turbulent kinetic energy for flames D and F are plotted in Figs. 2 and 3. The profiles of mean axial velocity are in good agreement with measurements, although

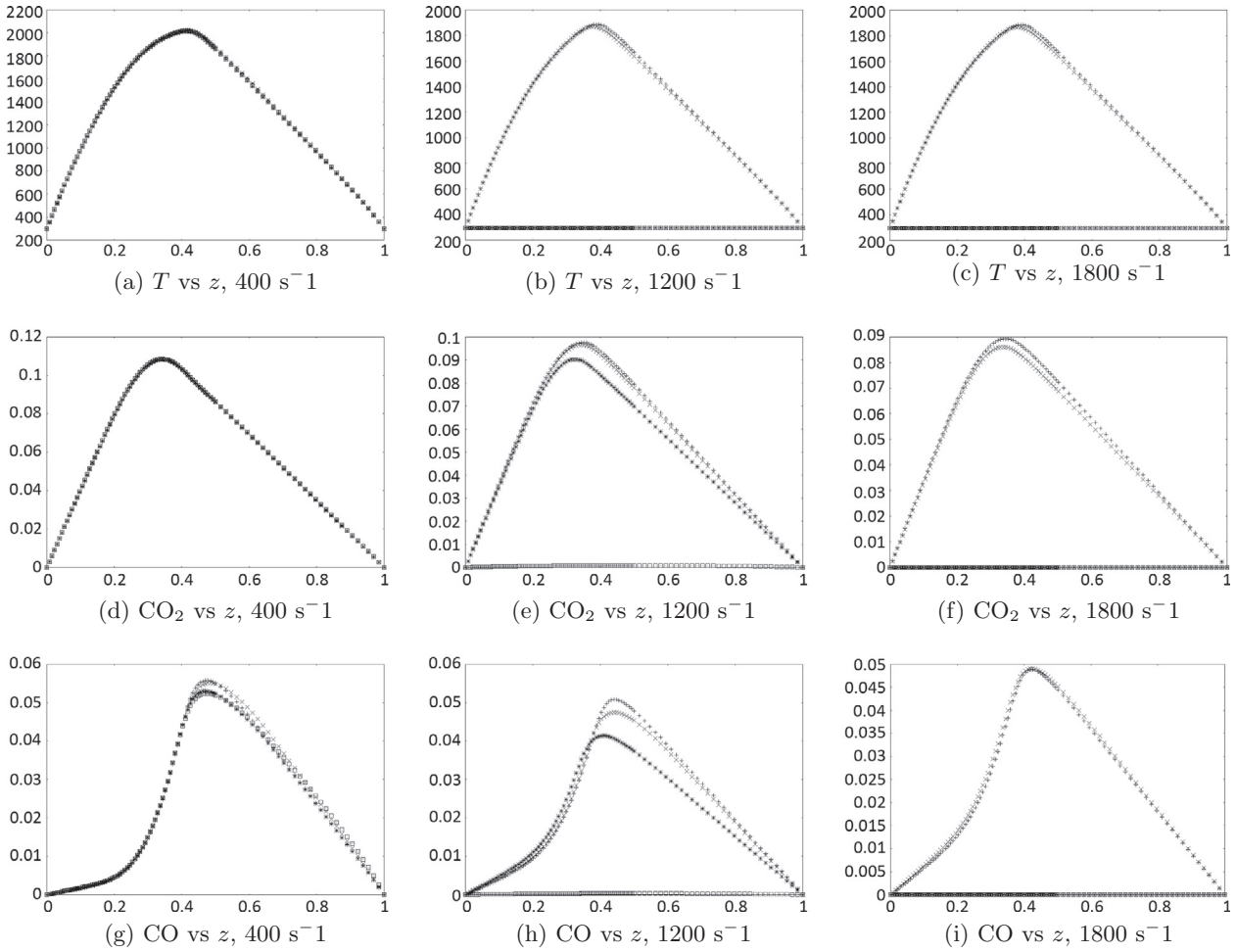


Fig. 1. Comparison of direct integration (+) with 18-constraint set (×), 16-constraint set (∗) and 14-constraint set (□) for a laminar flamelet with the Sandia inlet composition.

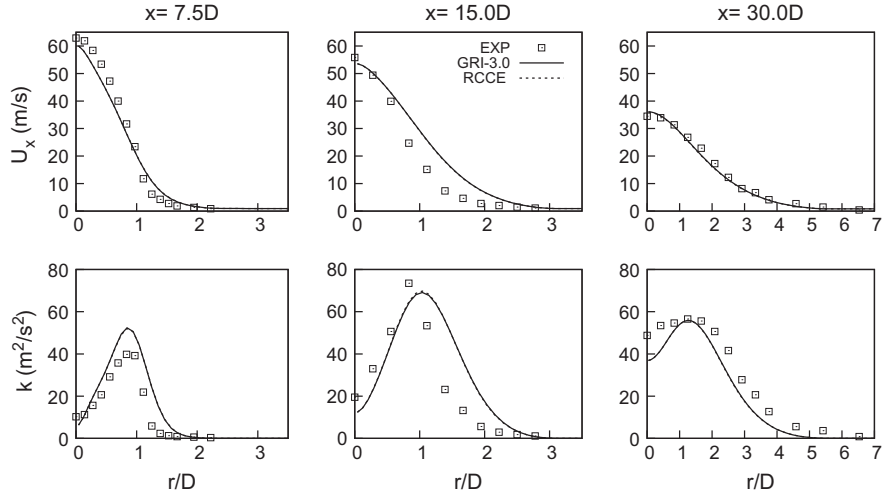


Fig. 2. Radial profiles of mean axial velocity and turbulent kinetic energy of flame D. Squares are measurements, solid lines are results from direct integration of GRI 3.0 and dashed lines are RCCE calculations.

there are some inaccuracies in the predicted turbulent kinetic energy.

The mean mixture fraction profiles are also reasonably accurate, showing that the shapes of the flames are reproduced correctly. An underprediction in centreline values of mean mixture fraction is notable, starting from $x = 25D$. The underprediction is visible near the centreline of the mean mixture fraction profile at $30D$ as in Fig. 4. On the other hand, the radial profiles of mean mixture

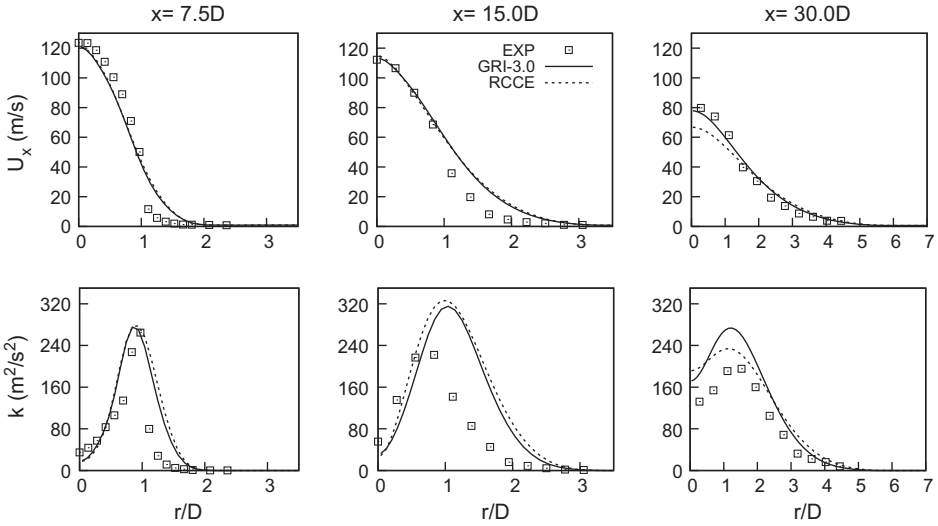


Fig. 3. Radial profiles of mean axial velocity and turbulent kinetic energy of flame F. Squares are measurements, solid lines are results from direct integration of GRI 3.0 and dashed lines are RCCE calculations.

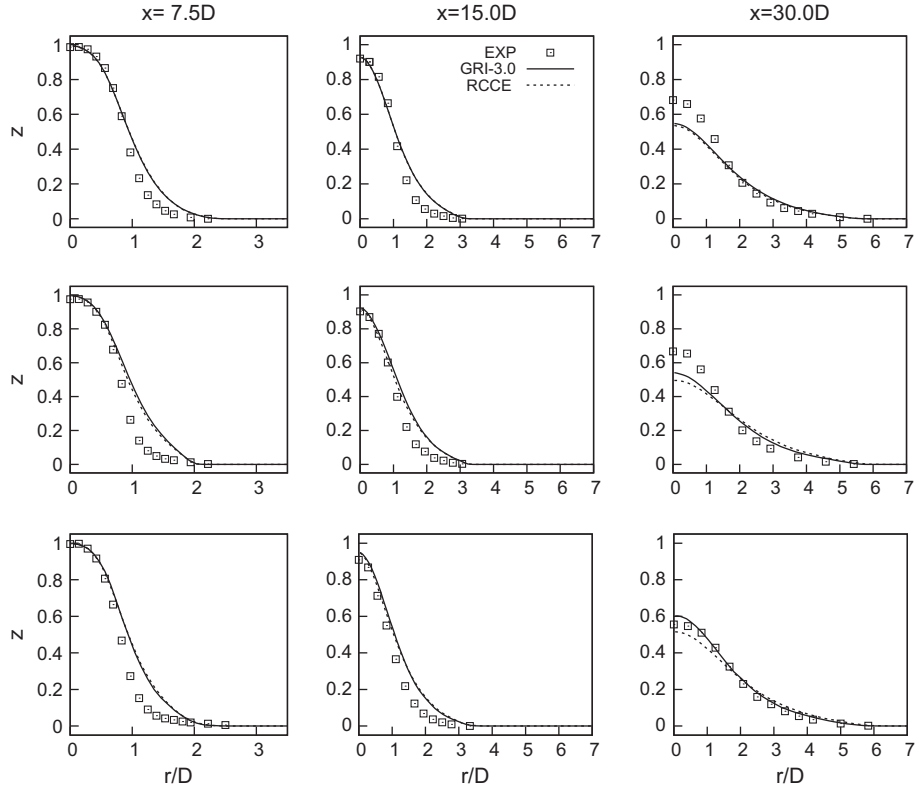


Fig. 4. Radial profiles of mean mixture fraction of the three flames. first row: flame D, second row: flame E and third row: flame F.

fraction up to $x = 15D$ are reasonably good near the centreline, with overpredictions in the outer regions of the 7.5*D* and 15*D* profiles indicating early radial overspreading of the jet.

5.2. Temperature and species profiles

The unconditional mean temperature and chemical species profiles of the three flames are shown in Figs. 5–10. In flame D (Figs. 5 and 6) the scalar fields are strongly correlated with the mixture fraction, hence the discrepancy in the mixture fraction affects the species and temperature profiles. The radial profiles of mean temperature in physical space (top row of Fig. 5) shows that discrepancies in mean temperature correspond to those in mixture fraction. This is visible in the fuel-lean side (outer region) in the 7.5*D* and 15*D* profiles and in the fuel-rich side (inner centreline region) in the 30*D* profile. Since the discrepancies in scalar fields are to a large extent induced by those in the mixture fraction predictions, mean species profiles were plotted against mixture fraction.

The most important observation is that the predictions of the RCCE simulations are nearly indistinguishable from those of direct

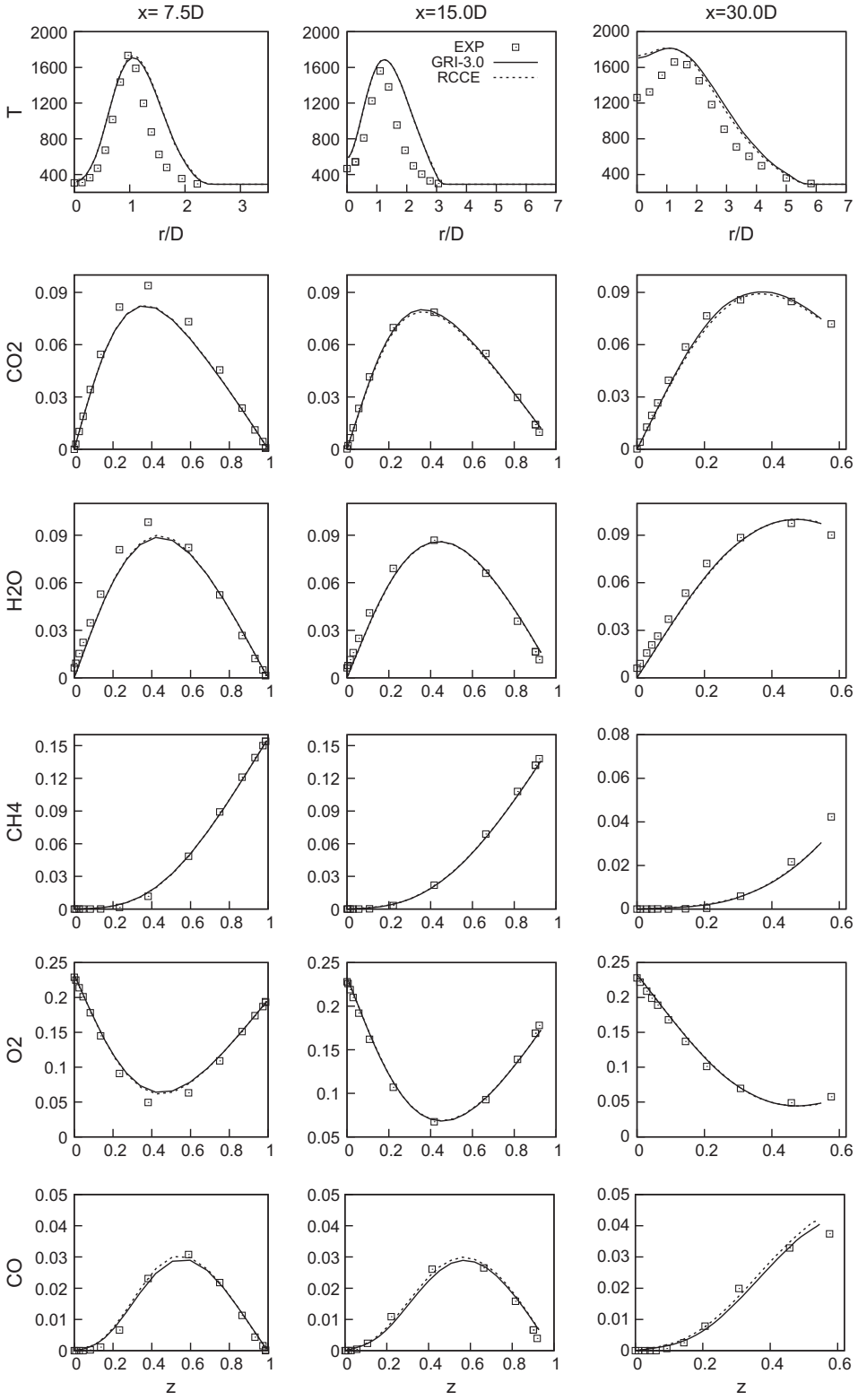


Fig. 5. Radial profiles of unconditional mean temperature in physical space and mean mass fractions of CO_2, H_2O, CH_4, O_2 and CO in mixture fraction space for flame D.

integration of the detailed mechanism, particularly for mean mixture fraction, temperature and the major species that were measured. Comparisons are also shown for the profiles of some minor species for which there are no measurements, and there again RCCE predictions shows very good agreement with the respective direct integration computations. Overall, the RCCE-reduced mechanism shows excellent ability to reproduce the finite-rate chemistry effects of the original mechanism in this flame.

The results for the unconditional scalar fields in flame E are shown in Figs. 7 and 8. Some of the observations that have been stated in the discussion of flame D are also relevant here, particularly those related to mean mixture fraction. There is some

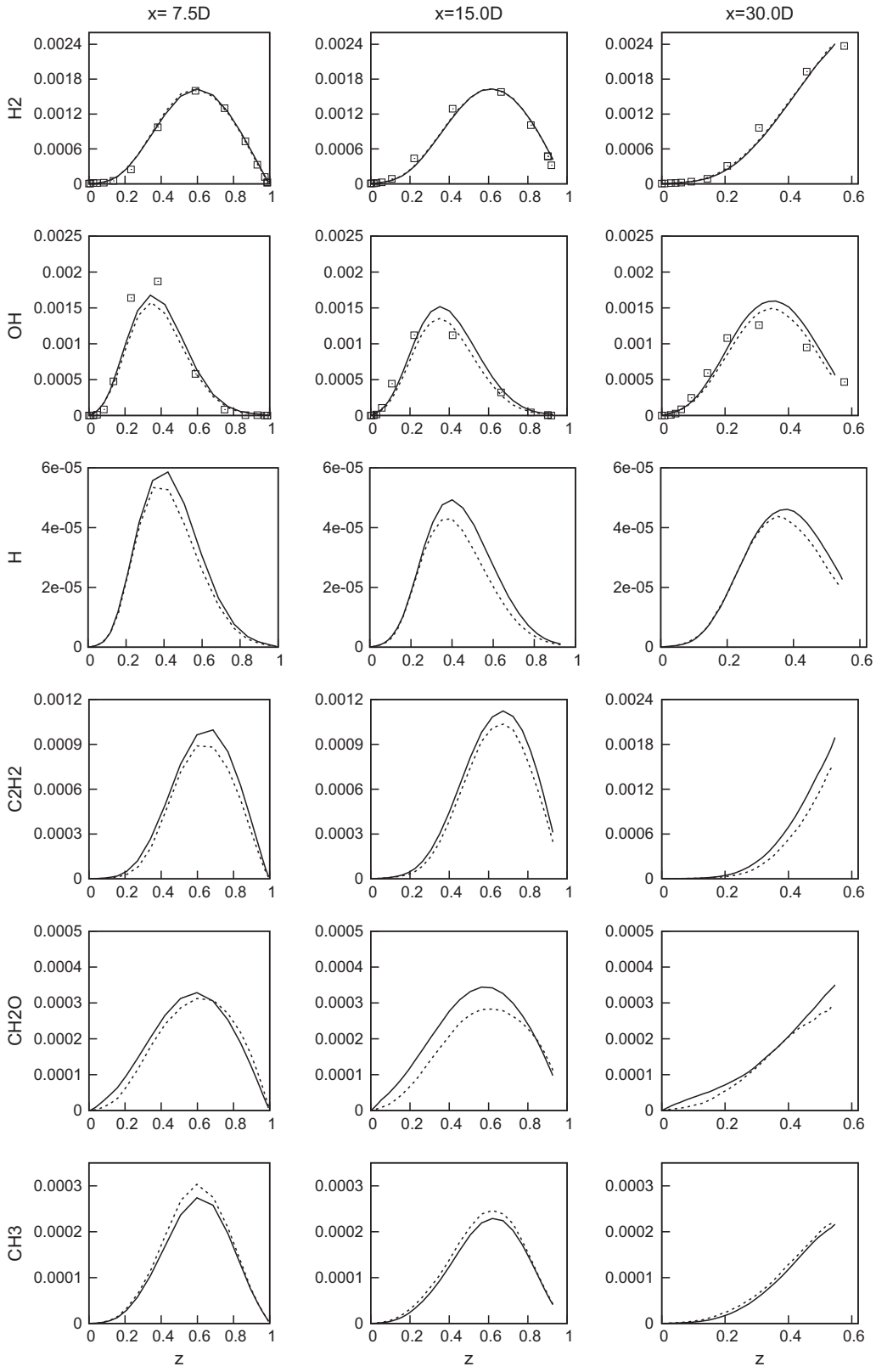


Fig. 6. Radial profiles of unconditional mean mass fractions of H_2, OH, H, C_2H_2, CH_2O and CH_3 in mixture fraction space for flame D.

discrepancy in the temperature and species profiles, particularly in locations where mean mixture fraction predictions are in disagreement with the measurements. In general, the unconditional scalar fields in flame E are reproduced with reasonable accuracy. Peak values of temperature and chemical products are relatively lower in this flame than in flame D, which is consistent with the trend shown in the measurements. In particular, the consumption rates of O_2 and CH_4 are reproduced with excellent accuracy.

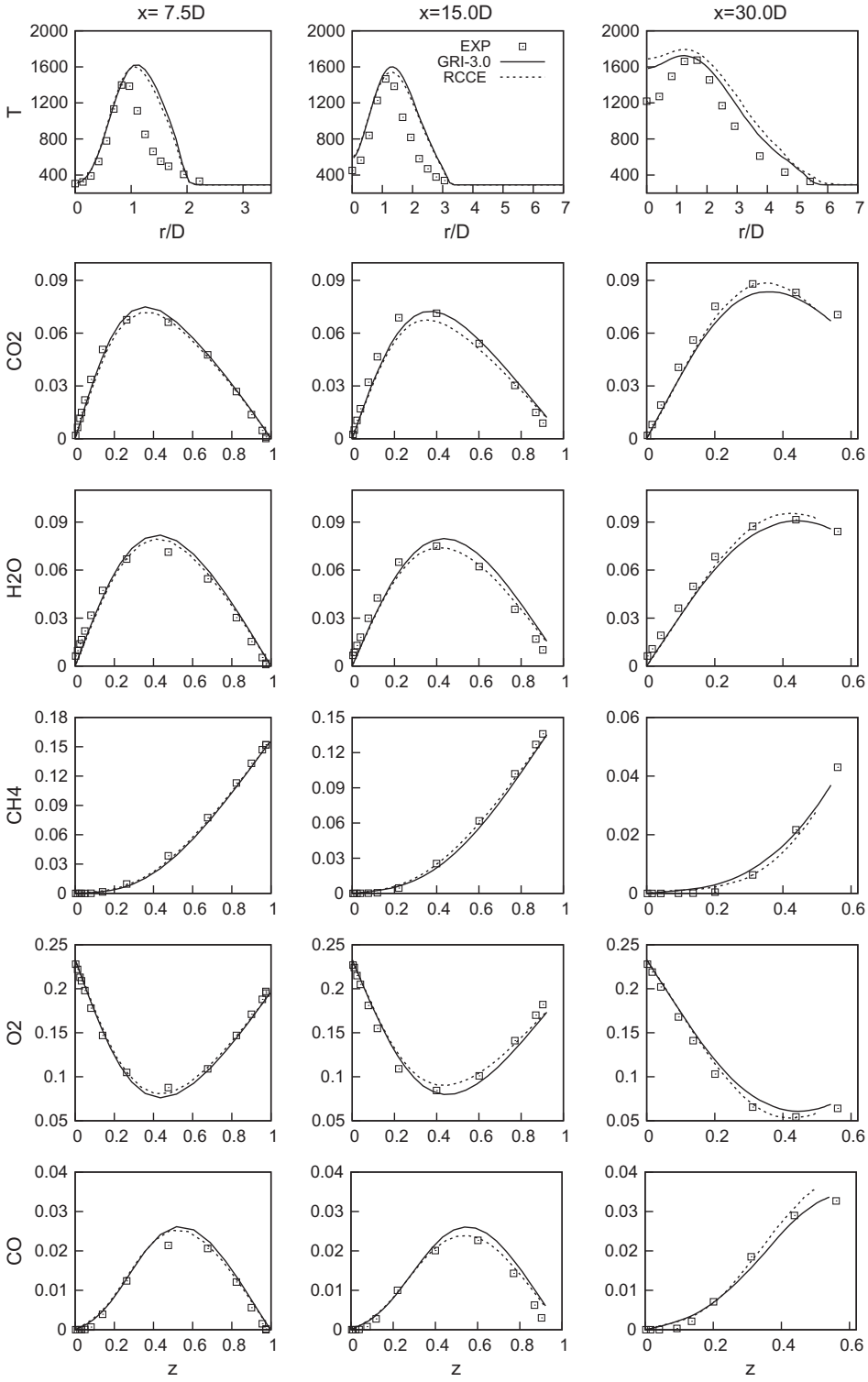


Fig. 7. Radial profiles of unconditional mean temperature in physical space and mean mass fractions of CO_2, H_2O, CH_4, O_2 and CO in mixture fraction space for flame E.

Remarkably, mean CO mass fraction is well predicted by both the direct integration of chemistry and RCCE at several locations. The commonly experienced overprediction of CO in fuel-rich regions in several previous studies is relatively small in the results obtained in this study. The RCCE-reduced mechanism once again shows excellent agreement with the detailed GRI 3.0 predictions, apart from some discrepancies in the prediction of the minor species at a somewhat higher level than that of flame D.

The results for the unconditional scalar fields in flame F are shown in the Figs. 5–10. The mixture fraction predictions in flame F are better than flames D and E in some regions. In particular, the mean mixture fraction profile at 30*D* is well predicted, in contrast to the other two flames where the values close to the centreline are considerably underpredicted in this axial location. The peak of mean temperature is overpredicted in the 7.5*D* and 15*D* but improved considerably at 30*D*. The

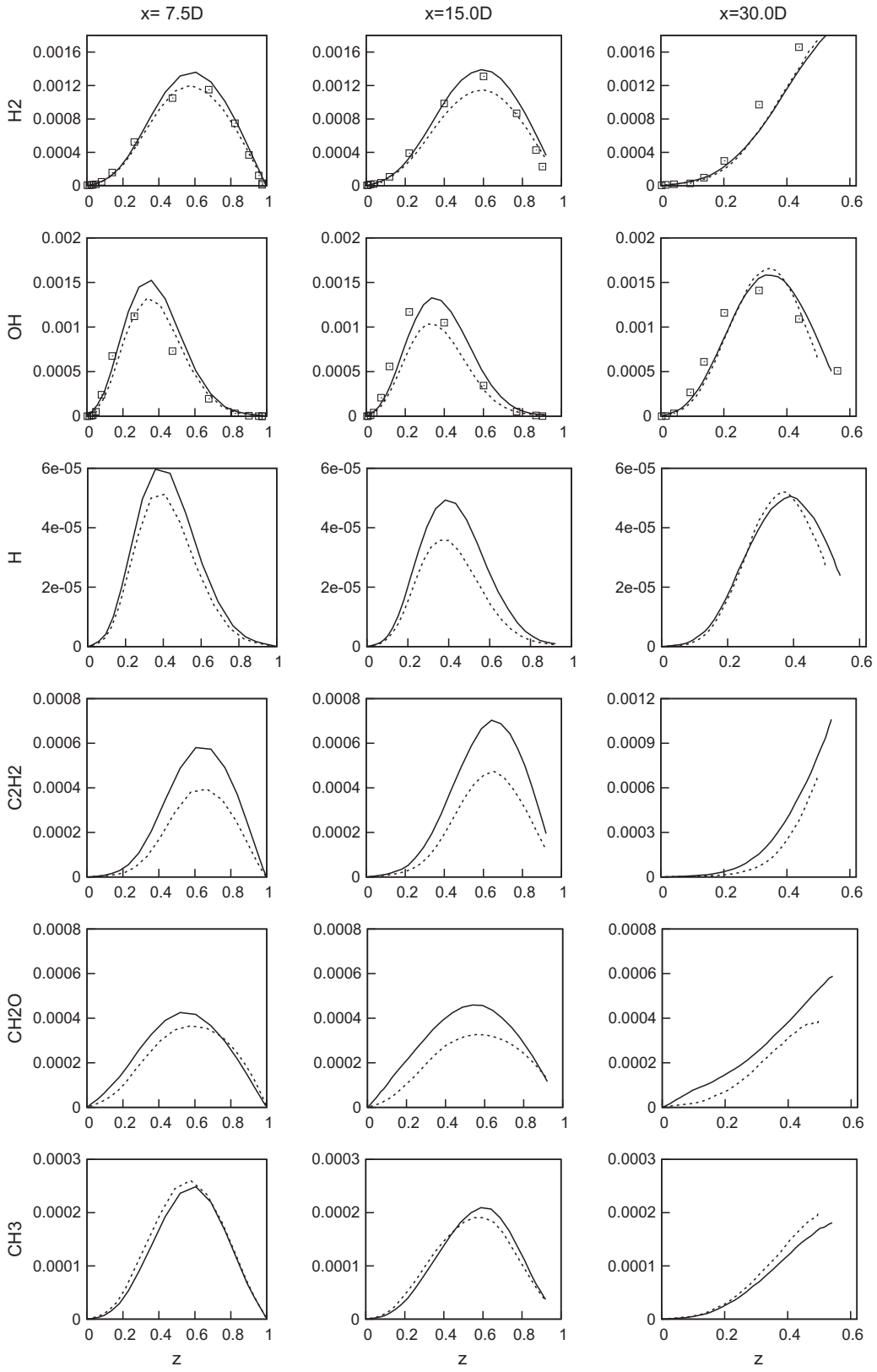


Fig. 8. Radial profiles of unconditional mean mass fractions of $H_2, OH, H, C_2H_2, CH_2O$ and CH_3 in mixture fraction space for flame E.

extinction at $15D$ is not fully captured, as it will be shown by the scatter plots. The temperature overprediction is accompanied with overprediction of consumption rates of reactants (O_2 and CH_4) in the flame zone at $x = 7.5D, x = 15D$, as well as of the major combustion products, and is due to the difficulty in producing the correct amount of extinction in flame F, which

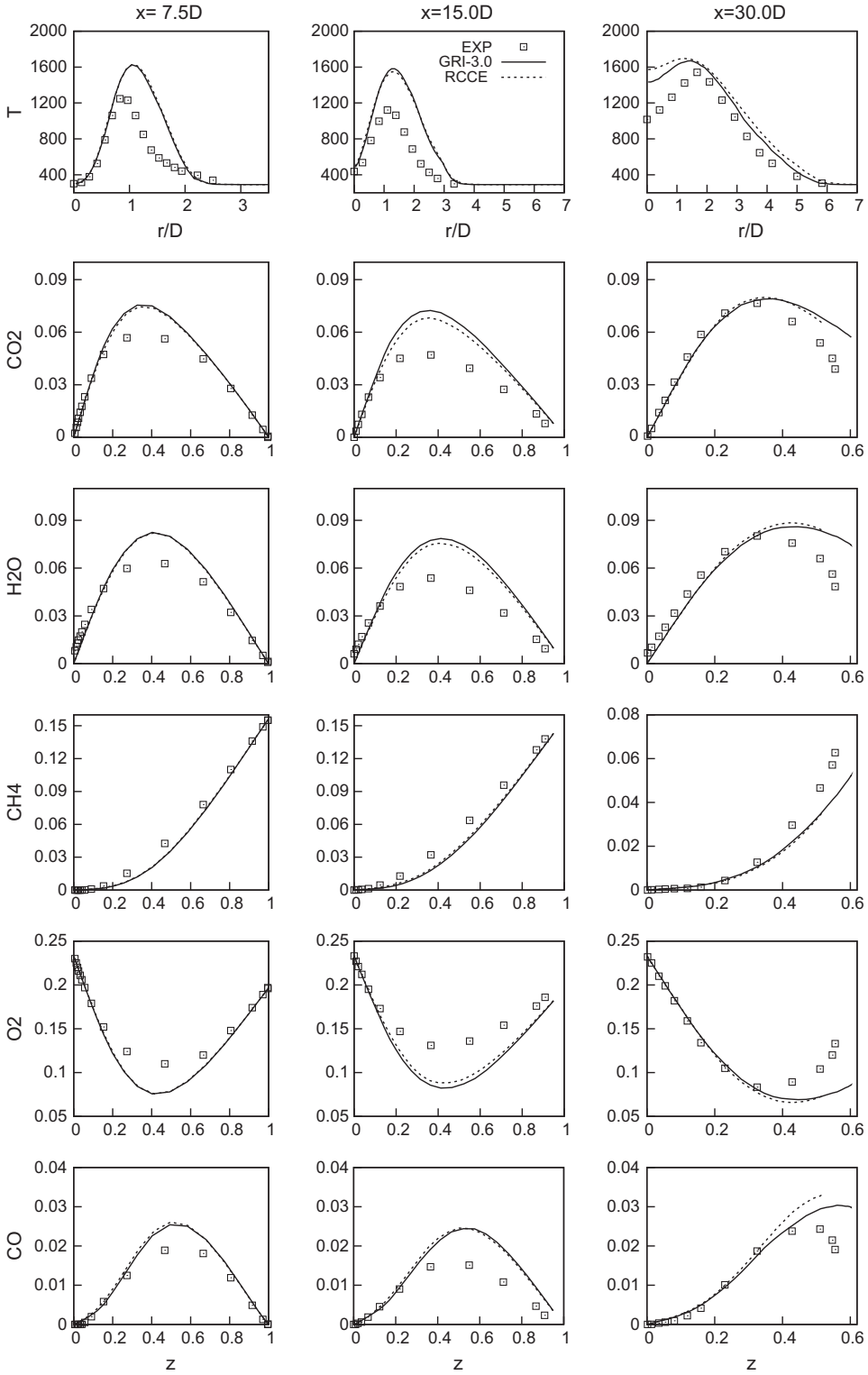


Fig. 9. Radial profiles of unconditional mean temperature in physical space and mean mass fractions of CO_2, H_2O, CH_4, O_2 and CO in mixture fraction space for flame F.

is a common feature of most studies of this flame. The comparison of RCCE results with direct integration shows very good agreement in most cases, following the trend exhibited by the previous two flames. The minor (non-measured) species show slightly better agreement in flame D, reflecting the less complex chemistry exhibited by this flame due to the lack of local extinction.

5.3. Scatter plots and micromixing

The effect of micromixing models on the prediction of extinction and reignition in these flames has been addressed by several studies such as [33,36,66]. Of particular relevance to us are the results of the IEM model reported in all three studies. The values of C_y adopted in these studies are higher than the value used in

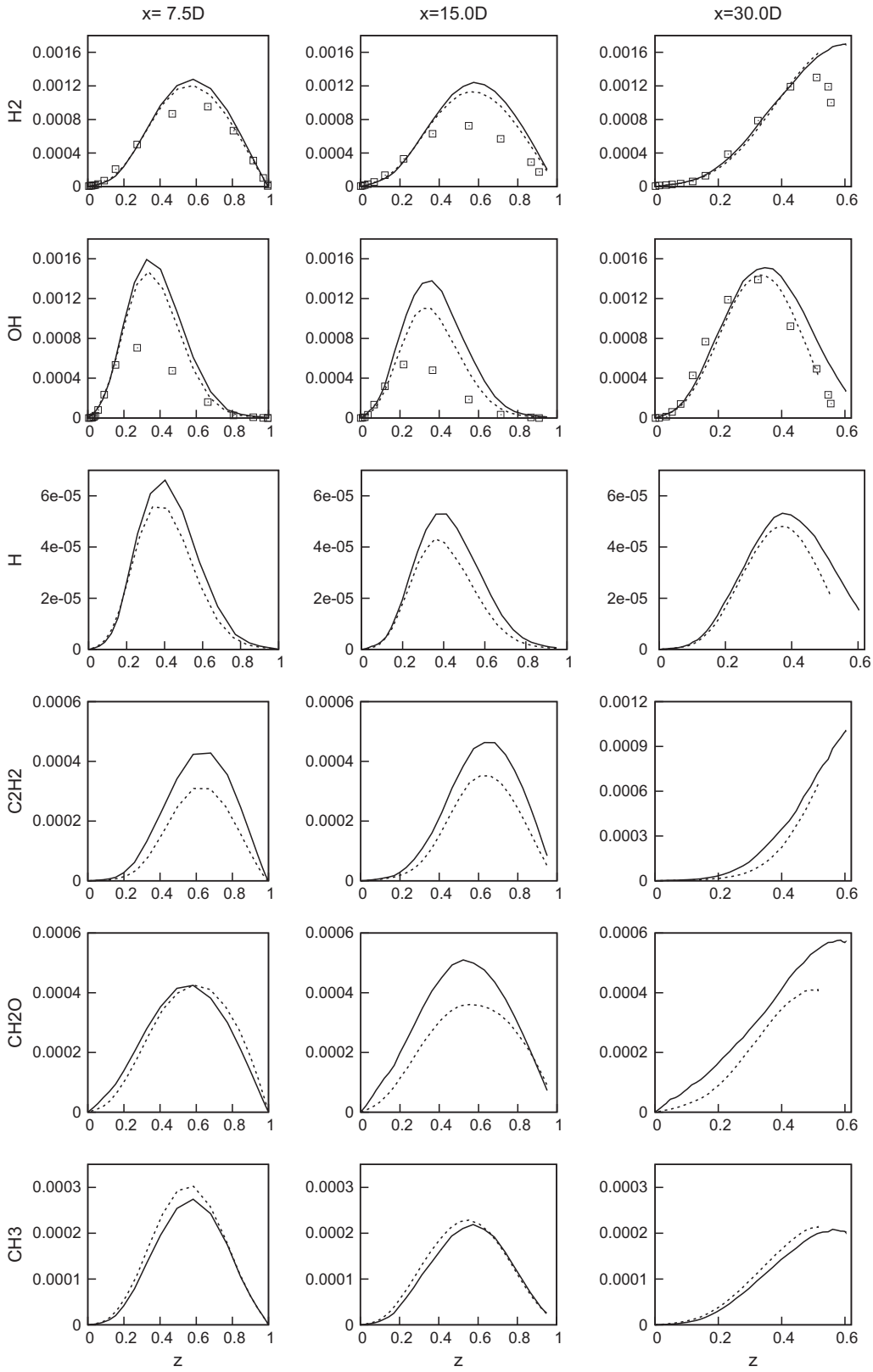


Fig. 10. Radial profiles of unconditional mean mass fractions of $H_2, OH, H, C_2H_2, CH_2O$ and CH_3 in mixture fraction space for flame F.

the present study, except for the flame D simulation of [36] where a value of 2.1 was used. Simulations with higher C_y values aid in obtaining a burning flame due to mixing enhancement, but result in underprediction of the mixture fraction variance. Preliminary calculations suggested that $C_y = 2.2$ is a good value for all three flames, and close to the theoretical one for the IEM model ($C_y = 2$).

The scatter plots of temperature for all three flames at stations 15*D* and 30*D* are shown in Figs. 11 and 12. Overall, the scatter plots

show that both the direct integration of the detailed mechanism and the RCCE-reduced mechanisms are capable of predicting an amount of extinction. Most important, regarding the objective of this study, is the fact that the results from RCCE and from direct integration of the full mechanism are in excellent agreement.

Many of the particles with lower temperature are likely to be particles that resulted from mixing between hot and cold particles, but have not resided enough time in the reaction zone to be ignited. These particles seem to diffuse away from the reaction zone due to excessive turbulent diffusion. Mixing between particles with very diverse compositions is improbable, but the IEM model lacks localness in composition space. Mixing and reaction should ideally result in a variety of ignition or extinction scenarios, which should result in spreading them over the allowable temperature and composition range.

In general, it can be concluded that agreement between direct integration and RCCE is very good but there is a considerable discrepancy in the comparison with experiments, which is due to the well-known shortcomings of the IEM mixing model. The latter are usually remedied in RANS-PDF methods by increasing the mixing rate coefficient or by the use of more advanced mixing models, while LES is more and more frequently being employed to improve the flow predictions and minimise the impact of the mixing model.

5.4. Comparison with other simulations of Sandia flames

Although the focus of this work is on the comparison of RCCE and direct integration, it is also useful to compare at this point the results of the present study with those of other studies of the Sandia flames, such as the LES-PDF study of Jones and Prasad [8], the RANS-PDF studies of Cao et al. [67,33], and the RANS-MMC studies of flame E by Wandel and Lindstedt [68] and of flame D by Vogiatzaki et al. [69]. Most of the studies, including the present one, predicted an insufficient amount of extinction in flame F at 15*D*, and consequently the peak temperature is around 400 K higher than the measured values. The only study that did not suffer from this overprediction is the simulations of Cao and Pope [67] with the EMST and GRI 3.0 in which radiative effects were not neglected. The overprediction of mean temperature in the extinction zone of flame F demonstrates the challenge of flame F to simulations in predicting the measured amount of extinction without causing blow-off of the flame.

Both the LES of [8,70] predict more extinction in flame F at 15*D* than in flame E. The scatter plots of the current study (Fig. 11) did not show noticeable difference between the flames E and F, even with the full GRI 3.0 mechanism, indicating the advantage of the LES over RANS approaches. There are some similarities between present scatter plots of flame D and those presented by Wang and Chen in [71] including the delay of reignition after $x = 30D$. Their methodology is similar to the current study in employing the GRI 3.0 mechanism in the context of the joint scalar PDF and RANS modelling, but they employed the EMST mixing model rather than the IEM.

On the other hand, in this work we obtained a remarkable level of accuracy of mean CO peak value, particularly in the fuel-rich regions of flames E and F. Mean CO profiles of flame E show less overprediction than the LES-PDF simulations of [8], the LES-FPV simulations of [38] and the RANS-MMC simulations of [68]. Furthermore, the amount of overprediction in the peak values of CO at the 30*D* axial location of flame F in [8] is larger than in this study. The correct prediction of mean CO is evident in the direct integrations, indicating the potential of the transported PDF

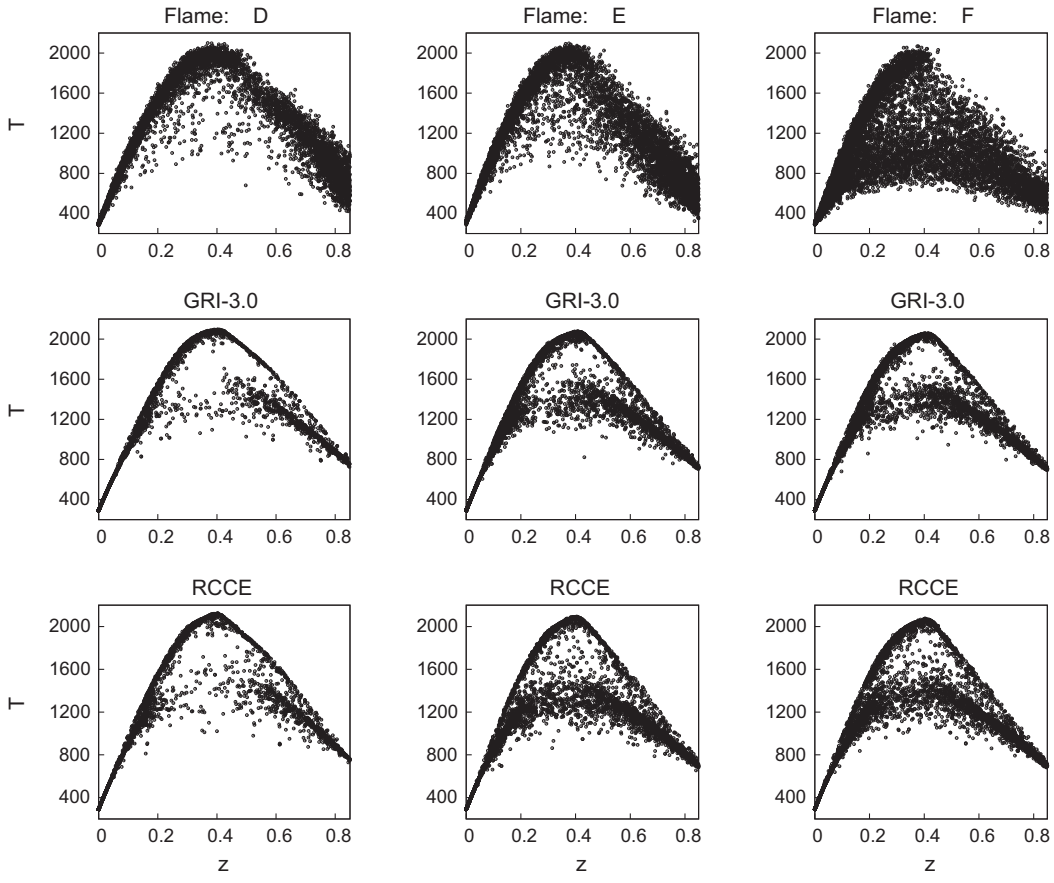


Fig. 11. Temperature scatter plot at x = 15D.

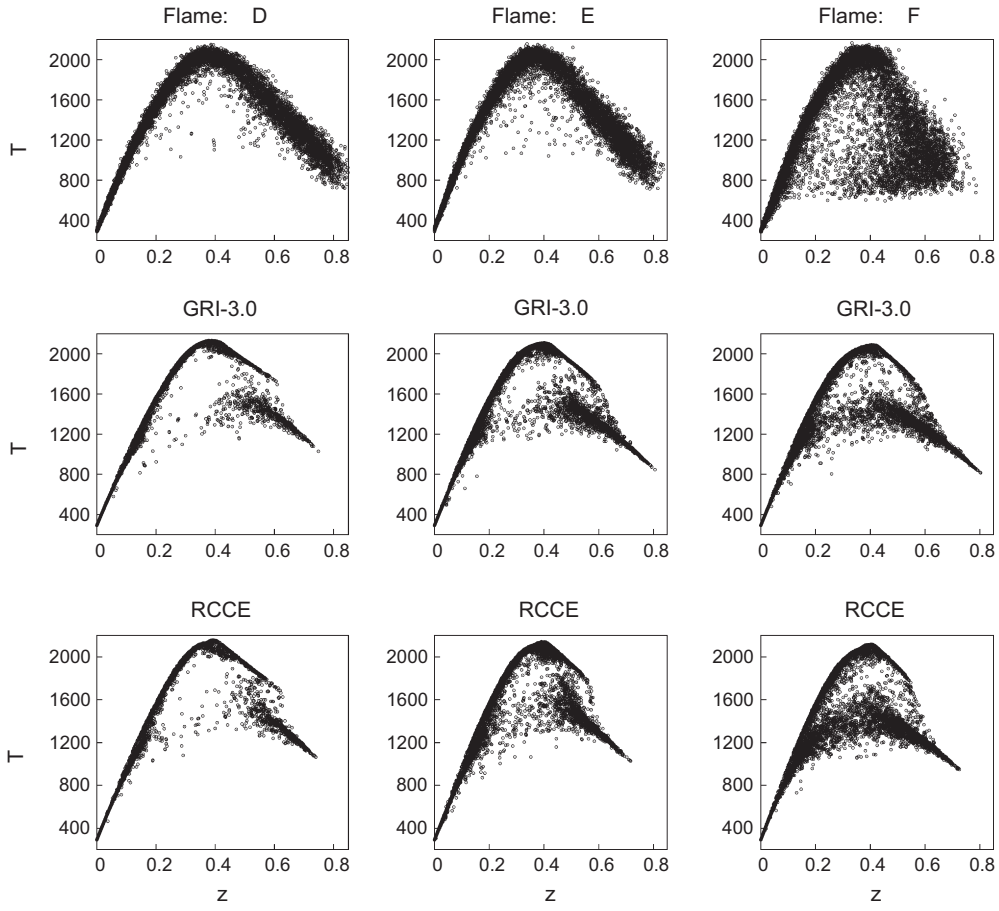


Fig. 12. Temperature scatter plot at $x = 30D$.

method, combined with the comprehensive chemistry found in the GRI 3.0 mechanism. What is more important with respect to the objective of this study, however, is the fact that the RCCE-reduced mechanism was able to retain this potential.

6. Conclusions

Mechanism reduction is key to the success of PDF methods, as chemistry computations are extremely expensive when carried out by detailed mechanisms. For large-scale PDF computations tabulation is the only practical way to introduce detailed chemistry (as in e.g. [27], but mechanism reduction is an essential prerequisite since the number of variables must be substantially reduced for tabulation to be feasible. RCCE is a systematic method of mechanism reduction that offers the flexibility of easy derivation and testing of reduced models, since the selection of slow/fast species enters as external input in the computational implementation. The objective of this paper was to assess the potential of RCCE as a physical assumption for mechanism reduction in turbulent flames. To this end, we performed real-time integration of the RCCE differential equations coupled with a transported PDF method for the Sandia D/E/F flames and compared their results with those from direct integration of a widely used detailed mechanism (GRI 3.0).

Computations were carried out with a RANS-PDF code employing the eddy-diffusivity $k-\varepsilon$ model for turbulence modelling and a Lagrangian Monte Carlo particle method for solving the joint-scalar PDF transport equation. The set of constraints for the RCCE was chosen based on flamelet simulations using detailed and RCCE-reduced chemistry at different strain rates. RCCE showed excellent ability in reproducing the finite-rate chemistry effects captured by the detailed mechanism in these turbulent jet flames, with the accuracy in the prediction of major and minor species' profiles reaching in most cases that of the detailed mechanism. The shape of the flames was reasonably well reproduced, with some discrepancies in mixture fraction caused by the eddy-diffusivity modelling. Scatter plots reproduced a reasonable amount of extinction and reignition present in the experiments, but more importantly the results of RCCE and direct integration were almost indistinguishable. Better yet predictions can be accomplished by employing a more advanced mixing model, or by LES, in which case the impact of the mixing model can be minimised through grid refinement. The main conclusion arising from this study, however, is that RCCE in its original form, i.e. direct integration of the RCCE ODEs coupled with a transported PDF method, is able to capture the chemical effects in turbulent flames at a level similar to that predicted by the detailed mechanism, while reducing its dimensionality and thus offering a sound basis for the development of tabulation approaches.

Acknowledgments

S. Elbahloul wishes to acknowledge the financial support that he received by the Libyan Ministry of Higher Education. S. Rigopoulos' work has been supported by the Royal Society.

References

[1] W.P. Jones, P. Lindstedt, Combust. Flame 73 (1998) 233–249.
[2] W. Jones, M. Kakhi, Combust. Flame 115 (1998) 210–229.
[3] J.-Y. Chen, R. Dibble, in: M. Smooke (Ed.), Reduced Kinetic Mechanisms and Asymptotic Approximations for Methane–Air Flames, Lecture Notes in Physics, vol. 384, Springer, Berlin Heidelberg, 1991, pp. 193–226.

[4] B. Yang, S. Pope, Combust. Flame 112 (1998) 85–112.
[5] V. Saxena, S.B. Pope, Symp. (Int.) Combust. 27 (1998) 1081–1086 (Twenty-Seventh Symposium (International) on Combustion Volume One).
[6] B. Liu, S. Pope, Combust. Theor. Model. 9 (2005) 549–568.
[7] R. Mustata, L. Valiño, C. Jimenez, W. Jones, S. Bondi, Combust. Flame 145 (2006) 88–104.
[8] W. Jones, V. Prasad, Combust. Flame 157 (2010) 1621–1636.
[9] C. Sung, C. Law, J.-Y. Chen, Combust. Flame 125 (2001) 906–919 (Cited By (since 1996)84).
[10] D. Goussis, S. Lam, Symp. (Int.) Combust. 22 (1988) 931–941.
[11] A. Massias, D. Diamantis, E. Mastorakos, D. Goussis, Combust. Flame 117 (1999) 685–708.
[12] T. Løvas, D. Nilsson, F. Mauss, Proc. Combust. Inst. 28 (2000) 1809–1815.
[13] A.S. Tomlin, T. Turányi, M.J. Pilling, Compr. Chem. Kinet. 35 (1997) 293–437.
[14] T. Lu, C.K. Law, Prog. Energy Combust. Sci. 35 (2009) 192–215.
[15] J. Keck, D. Gillespie, Combust. Flame 17 (1971) 237–241.
[16] J.C. Keck, Prog. Energy Combust. Sci. 16 (1990) 125–154.
[17] V. Yousefian, Combust. Flame 115 (1998) 66–80.
[18] W. Jones, S. Rigopoulos, Proc. Combust. Inst. 30 (2005) 1325–1331.
[19] W.P. Jones, S. Rigopoulos, Combust. Flame 142 (2005) 223–234.
[20] W.P. Jones, S. Rigopoulos, Combust. Theor. Model. 11 (2007) 755–780.
[21] S. Rigopoulos, T. Løvås, Proc. Combust. Inst. 32 (2009) 569–576.
[22] M. Janbozorgi, S. Ugarte, H. Metghalchi, J.C. Keck, Combust. Flame 156 (2009) 1871–1885.
[23] Z. Ren, G.M. Goldin, V. Hiremath, S.B. Pope, Combust. Theor. Model. 15 (2011) 827–848.
[24] V. Hiremath, Z. Ren, S.B. Pope, Combust. Flame 158 (2011) 2113–2127.
[25] S. Navarro-Martinez, S. Rigopoulos, Flow Turbul. Combust. 87 (2011) 407–423.
[26] S. Navarro-Martinez, S. Rigopoulos, Flow Turbul. Combust. 89 (2012) 311–328.
[27] A. Chatzopoulos, S. Rigopoulos, Proc. Combust. Inst. 34 (2013) 1465–1473.
[28] Z. Ren, G.M. Goldin, V. Hiremath, S.B. Pope, Fuel 105 (2013) 636–644.
[29] V. Hiremath, S.R. Lantz, H. Wang, S.B. Pope, Proc. Combust. Inst. 34 (2013) 205–215.
[30] R. Lindstedt, S. Louloudi, Proc. Combust. Inst. 29 (2002) 2147–2154.
[31] Q. Tang, J. Xu, S.B. Pope, Proc. Combust. Inst. 28 (2000) 133–139.
[32] J. Xu, S. Pope, Combust. Flame 123 (2000) 281–307.
[33] R.R. Cao, H. Wang, S.B. Pope, Proc. Combust. Inst. 31 (2007) 1543–1550.
[34] R. Lindstedt, S. Louloudi, J. Driscoll, V. Sick, Flow, Turbul. Combust. 72 (2004) 407–426.
[35] R. Lindstedt, S. Louloudi, E. Vaos, Proc. Combust. Inst. 28 (2000) 149–156.
[36] J. Jaishree, D.C. Haworth, Combust. Theor. Model. 16 (2012) 435–463.
[37] H. Pitsch, H. Steiner, Phys. Fluids 12 (2000) 2541–2554.
[38] M. Ihme, H. Pitsch, Combust. Flame 155 (2008) 90–107.
[39] A. Kronenburg, M. Kostka, Combust. Flame 143 (2005) 342–356 (Special Issue to Honor Professor Robert W. Bilger on the Occasion of His Seventieth Birthday).
[40] A. Garmory, E. Mastorakos, Proc. Combust. Inst. 33 (2011) 1673–1680.
[41] A. Garmory, E. Mastorakos, Int. J. Heat Fluid Flow 39 (2013) 53–63.
[42] W. Jones, B. Launder, Int. J. Heat Mass Transfer 15 (1972) 301–314.
[43] W. Jones, B. Launder, Int. J. Heat Mass Transfer 16 (1973) 1119–1130.
[44] E. O'Brien, in: P. Libby, F. Williams (Eds.), Turbulent Reacting Flows, Topics in Applied Physics, vol. 44, Springer, Berlin Heidelberg, 1980, pp. 185–218.
[45] S. Pope, Prog. Energy Combust. Sci. 11 (1985) 119–192.
[46] D. Haworth, Prog. Energy Combust. Sci. 36 (2010) 168–259.
[47] J. Villermaux, J.C. Devillon, in: Second International Symposium on Chemical Reaction Engineering, Elsevier, New York, 1972, pp. 1–13.
[48] C. Dopazo, E. O'Brien, Acta Astronaut. 1 (1974) 1239–1266.
[49] W. Jones, in: B. Launder, N. Sandham (Eds.), Closure Strategies for Turbulent and Transitional Flows, Cambridge University Press, 2002.
[50] R.S. Barlow, J.H. Frank, Proc. Combust. Inst. 27 (1998) 1087–1095.
[51] R.S. Barlow, J.H. Frank, A.N. Karpetis, J.-Y. Chen, Combust. Flame 143 (2005) 433–449.
[52] C. Schneider, A. Dreizler, J. Janicka, E. Hassel, Combust. Flame 135 (2003) 185–190.
[53] A. Masri, R. Dibble, R. Barlow, Prog. Energy Combust. Sci. 22 (1997) 307–362.
[54] G.D. Veroli, S. Rigopoulos, AIChE J. 56 (2010) 878–892.
[55] G.Y. Di Veroli, S. Rigopoulos, Phys. Fluids 23 (2011).
[56] W. Jones, BOFFIN: A Computer Program for Flow and Combustion in Complex Geometries, 1994.
[57] B.V. Leer, J. Comput. Phys. 14 (1974). 361-270.
[58] W. Jones, in: P. Libby, F. Williams (Eds.), Turbulent Reactive Flows, Academic Press, New York, 1994, pp. 309–373.
[59] P. Escudier, The Distribution of the Mixing Length in Turbulent Flows Near Walls, Technical Note: Mechanical Engineering Department, Imperial College of Science and Technology, Mechanical Engineering Department, 1965.
[60] B. Merci, E. Dick, J. Vierendeels, C.D. Langhe, Int. J. Numer. Methods Heat Fluid Flow 12 (2002) 65–80.
[61] K. Morgan, T. Hughes, C. Taylor, Appl. Math. Model. 1 (1977) 395–400.
[62] R. Barlow, J. Frank, Piloted CH_4/Air Flames C, D, E, and F – Release 2.1, 2007 <http://www.sandia.gov/TNF/pilotedjet.html>.
[63] T. Løvås, S. Navarro-Martinez, S. Rigopoulos, Proc. Combust. Inst. 33 (2011) 1339–1346.
[64] C. Sung, C. Law, J.-Y. Chen, Symp. (Int.) Combust. 27 (1998) 295–304 (Twenty-Seventh Symposium (International) on Combustion Volume One).
[65] C. Sung, C. Law, J.-Y. Chen, Combust. Sci. Technol. 156 (2000) 201–220.
[66] H. Wang, S.B. Pope, Combust. Theor. Model. 12 (2008) 857–882.
[67] R.R. Cao, S.B. Pope, Combust. Flame 143 (2005) 450–470.
[68] A.P. Wandel, R.P. Lindstedt, Proc. Combust. Inst. 34 (2013) 1365–1372.
[69] K. Vogiatzaki, A. Kronenburg, S. Navarro-Martinez, W. Jones, Proc. Combust. Inst. 33 (2011) 1523–1531.
[70] Y. Ge, M. Cleary, A. Klimenko, Proc. Combust. Inst. 34 (2013) 1325–1332.
[71] H. Wang, Y. Chen, Chem. Eng. Sci. 59 (2004) 3477–3490.